

Characterization of neuropathology in ovine CLN5 and CLN6 neuronal ceroid lipofuscinoses (Batten disease)

Nadia L. Mitchell¹  | Katharina N. Russell¹ | Graham K. Barrell¹  |
Imke Tammen²  | David N. Palmer¹ 

¹Faculty of Agriculture and Life Sciences, Lincoln University, Lincoln, New Zealand

²Faculty of Science, Sydney School of Veterinary Science, The University of Sydney, Camperdown, New South Wales, Australia

Correspondence

Nadia L. Mitchell, Faculty of Agriculture and Life Sciences, Lincoln University, PO Box 85084, Lincoln 7647, New Zealand.
Email: Nadia.Mitchell@lincoln.ac.nz

Funding information

Batten Disease Support and Research Association

Abstract

Sheep with naturally occurring CLN5 and CLN6 forms of neuronal ceroid lipofuscinoses (Batten disease) share the key clinical features of the human disease and represent an ideal model system in which the clinical efficacy of gene therapies is developed and test. However, it was first important to characterize the neuropathological changes that occur with disease progression in affected sheep. This study compared neurodegeneration, neuroinflammation, and lysosomal storage accumulation in CLN5 affected Borderdale, CLN6 affected South Hampshire, and Merino sheep brains from birth to end-stage disease at ≤ 24 months of age. Despite very different gene products, mutations, and subcellular localizations, the pathogenic cascade was remarkably similar for all three disease models. Glial activation was present at birth in affected sheep and preceded neuronal loss, with both spreading from the visual and parieto-occipital cortices most prominently associated with clinical symptoms to the entire cortical mantle by end-stage disease. In contrast, the subcortical regions were less involved, yet lysosomal storage followed a near-linear increase across the diseased sheep brain with age. Correlation of these neuropathological changes with published clinical data identified three potential therapeutic windows in affected sheep—presymptomatic (3 months), early symptomatic (6 months), and a later symptomatic disease stage (9 months of age)—beyond which the extensive depletion of neurons was likely to diminish any chance of therapeutic benefit. This comprehensive natural history of the neuropathological changes in ovine CLN5 and CLN6 disease will be integral in determining what impact treatment has at each of these disease stages.

KEYWORDS

Batten disease, lysosomal storage, neurodegeneration, neuroinflammation, pathogenic cascade, sheep

This is an open access article under the terms of the [Creative Commons Attribution](https://creativecommons.org/licenses/by/4.0/) License, which permits use, distribution and reproduction in any medium, provided the original work is properly cited.

© 2023 The Authors. *Developmental Neurobiology* published by Wiley Periodicals LLC.

1 | INTRODUCTION

The neuronal ceroid lipofuscinoses (NCLs; Batten disease) are a group of rare, fatal lysosomal storage diseases. Mutations in any 1 of 13 genes (designated *CLN1-8*, *10-14*) are proposed to cause NCL (Butz et al., 2020) (www.ucl.ac.uk/ncl) yet they all result in the near-ubiquitous intracellular accumulation of proteinaceous lysosome-derived storage bodies (Palmer, 2015), widespread gliosis and regionally specific neurodegeneration, which generalizes to severe brain atrophy (Mole et al., 2011). Patients suffer from progressive psychomotor deterioration, retinal degeneration resulting in loss of vision, seizures, and premature death between 7 years of age and early adulthood (Mole et al., 2011).

Presently, there are no cures, but therapeutic attempts are underway. A promising enzyme replacement therapy has been globally approved for CLN2 disease (Schulz et al., 2018), and clinical trials of gene therapies for CLN3, 5, 6, 7, and 8 disease are occurring or in development (Kohlschütter et al., 2019; Liu et al., 2020). Most of the preclinical studies have occurred in rodents but naturally occurring sheep (*Ovis aries*) models of NCL have advantages for such studies. Their comparable size, humanlike gyrencephalic brain, and relative longevity render them better translational candidates to test therapies and clinical dosing regimens for pediatric neurodegenerative diseases over longer timescales. Furthermore, the United States Food and Drug Administration (FDA) recommends that efficacy in preclinical studies be shown in more than one animal species (Singh & Seed, 2021), including “more biologically relevant” larger animal models to bridge the gaps in small model research (Eaton & Wishart, 2017).

Three naturally occurring ovine NCL research flocks in Australasia (Australia and New Zealand) are the representative of two defective NCL protein classes and subcellular localizations. A substitution mutation (c.571 + 1G > A) in the *CLN5* gene in New Zealand Borderdale sheep results in a truncated soluble lysosomal CLN5 protein (OMIA 001482-9940) (Frugier et al., 2008). Two different mutations have been detected in the ovine *CLN6* gene, indicated to code for an intracellular endoplasmic reticulum (ER)-resident membrane bound protein (Heine et al., 2004; Mole et al., 2004). A large deletion and 1 bp insertion (g.-251_+150del and g.+150_151insC) in New Zealand South Hampshire sheep and a missense mutation (c.184C > T; p.Arg62Cys) in Australian Merino sheep result in ovine CLN6 disease models (OMIA 001443-9940) (Mohd Ismail, 2014; Tammen et al., 2006). The molecular function of the CLN5 and CLN6 proteins is still unclear; however, both appear to be required for the biogenesis and function of lysosomes. CLN5 has been postulated to function enzymatically as a glycoside hydrolase or *S*-depalmitoylase (Huber & Mathavarajah, 2018; Luebben et al., 2022), whereas CLN6 is believed to form an EGRESS

complex with CLN8 to transport newly synthesized lysosomal proteins from the ER to the Golgi (Bajaj et al., 2020). Yet, despite very different gene products, mutations, subcellular protein localizations, and potential protein functions, CLN5 and CLN6 affected sheep exhibit a similar disease onset and progression that mimics the main clinical features of the human condition and includes visual loss from 7 to 14 months, progressive neurological symptomatology, lysosomal storage, and premature death before 24 months of age (Cook et al., 2002; Jolly et al., 1989, 2002; Mayhew et al., 1985).

Detailed quantitative information about the neuropathological changes in human NCL is restricted to biopsy and/or end-stage autopsy findings, whereas the temporal and spatial neuropathological cascades in NCL are easily studied in well-characterized animal models. The causative mutations of these ovine CLN5 and CLN6 NCLs have been identified and molecular genetic diagnoses developed (Frugier et al., 2008; Tammen et al., 2006), so affected sheep can be genotyped at birth and the progression of pathological changes in the ovine disease assessed from a perinatal stage, with no overt symptoms, through to humane terminal disease at 18–24 months of age. Systematic studies have already provided a detailed quantitative assessment of storage body accumulation, glial activation, and cortical atrophy in CLN6 affected South Hampshire sheep brains (Kay et al., 2006; Oswald et al., 2005, 2008). This study aimed to replicate those analyses to document the pathological changes within the CLN5 Borderdale and CLN6 Merino diseased sheep brain to the same extent.

Finally, gene therapy represents a promising treatment option for CLN5 and CLN6 Batten disease. Understanding the spatiotemporal development of disease will be integral in determining the optimal window for therapeutic intervention and if a treatment has impacted on neuronal loss, neuroinflammation, or lysosomal storage.

2 | MATERIALS AND METHODS

2.1 | Animals

Homozygous CLN6 affected Merino (Mer CLN6^{-/-}), South Hampshire (SH CLN6^{-/-}), and CLN5 affected Borderdale (CLN5^{-/-}) sheep were diagnosed at birth and maintained at the University of Sydney or Lincoln University as described (Frugier et al., 2008; Tammen et al., 2006).

Brains from two to five affected animals of each genotype, aged newborn (0–12 days), 3, 6, 9, 12, 15, 18, and 24 months, were included in this study together with age-matched clinically healthy heterozygous controls. Animals of mixed sex were included in both groups as no gender-based difference in disease development has been noted for any of the sheep breeds. It was not possible to source newborn or

15-month-old affected South Hampshire brains or newborn, 3, 9, or 24-month-old affected Merino brains. Historical brain weight data were collected from over 250 control and affected sheep of mixed sex.

All studies are reported in accordance with the ARRIVE guidelines. Animal procedures complied with the New Zealand Animal Welfare Act (1999), the Australian Code of Practice for the Care and Use of Animals for Scientific Purposes, and National Institutes of Health (NIH) guidelines, under the approval of the Lincoln University and University of Sydney animal ethics committees.

2.2 | Tissue preparation and histology

Borderdale and South Hampshire sheep were euthanized by penetrating captive bolt stunning and immediate exsanguination and the brain perfusion-fixed in situ via the carotid artery with 10% formalin, pH 7.4 (Oswald et al., 2005). Intact brains were removed, weighed, bisected at the sagittal midline, and left in fixative, 1 week, 4°C. After equilibration in cryoprotective solution (10% ethylene glycol, 20% sucrose in 0.9% NaCl), 4°C, for 5 days, brain hemispheres were frozen at -80°C.

Merino sheep were euthanized by an intravenous lethal injection of 0.5 mL/kg sodium pentobarbitone (Lethabarb, Virbac Animal Health, Australia) or through deep intravenous sedation with 0.5 mg/mL diazepam and 5 mg/kg ketamine (Troy Animal Healthcare, Australia) followed by immediate exsanguination. Brains were perfusion fixed as above or immersion fixed in 10% formalin in 0.9% NaCl, pH 7.4 for extended periods, and then transported to New Zealand for equilibration and processing.

Sequential 50 μ m sagittal brain sections were cut through the mediolateral extent of one hemisphere using a freezing sliding microtome (Microm International, Walldorf, Germany). Sections were collected, one per well, into 96-well plates containing cryopreservative (30% ethylene glycol, 15% sucrose, and 0.05% sodium azide in phosphate buffered saline solution [PBS], pH 7.4) and stored at -20°C until required. Matched series of sections from each animal were selected from five sagittal levels for all subsequent analyses (Oswald et al., 2005).

For Nissl and Luxol fast blue (LFB) histological staining, sections from each level were mounted in chrome alum solution (0.5% gelatine and 0.05% chromium potassium sulfate) on microscope slides, air-dried, dehydrated through an ethanol gradient, and cleared in xylene. One set was rehydrated through the ethanol gradient, equilibrated in water, and incubated, 10 min, in Nissl solution (0.05% cresyl violet acetate C5042; Sigma-Aldrich, St. Louis, MO, USA, 0.05% acetic acid in water) at 37°C and rinsed in water. Sections were then dehydrated, cleared in xylene, and coverslipped

with DPX (BDH, Poole, UK). The other set was equilibrated in ethanol, incubated, 24 h at 40°C in an airtight container in LFB staining solution (0.1% Solvent Blue 38, S3382; Sigma-Aldrich, 95% ethanol), rinsed in 70% ethanol, 3 min, incubated in 0.05% lithium carbonate, 10 min, taken back through the alcohol gradient to xylene, then mounted in DPX.

2.3 | Immunohistochemistry

Sections were stained with rabbit anti-cow glial fibrillary acidic protein (GFAP; 1:5000, Z0334, Dako, Ely, UK) for astrocytes; a biotinylated form of the α -D-galactose specific isolectin I-B4 from *Griffonia simplicifolia* (GSB4, 1:500; B-1205; Vector Laboratories, Burlingame, CA, USA) for microglia; and CLN5 or CLN6 antibodies (1:500; R19122 and 19121 respectively; Viraquest Inc, North Liberty, IA, USA) for endogenous NCL protein expression. All antibodies were diluted in 10% normal goat serum (NGS, Life Technologies NZ Ltd, Auckland, New Zealand) in PBS, pH 7.4, containing 0.3% Triton X-100 (PBST). For each antigen, sections from all genotypes, ages, and levels were batch processed simultaneously.

Thawed sections were blocked with either 1% H₂O₂ in PBS (GFAP, CLN5, CLN6) or 1% H₂O₂ in 50% methanol in PBS (GSB4), 30 min, room temperature. Sections were then pre-incubated in 15% NGS in PBST prior to overnight incubation at 4°C in primary antibody/lectin. Immunoreactivity was detected using biotinylated goat anti-rabbit IgG (1:1000; B7389; Sigma-Aldrich), 2 h, room temperature, followed by ExtrAvidin peroxidase (1:1000; E2886; Sigma-Aldrich) for 2 h at room temperature. Staining was visualized by incubation in 0.05% 3,3'-diaminobenzidine (DAB; D5637; Sigma-Aldrich) and 0.01% H₂O₂ in PBS, 7 min (GFAP, CLN5, CLN6) or 5 min (GSB4). Negative control sections, in which either the primary or secondary antibody was omitted, were included in all staining runs. Sections were mounted in chrome alum solution, air-dried, dehydrated in 100% ethanol, cleared in xylene, and coverslipped with DPX. Further unstained sections were mounted as above, air-dried, and coverslipped with glycerol for fluorescent microscopy.

2.4 | Microscopy and quantitation

Digital images of stained sections were obtained with a Nikon Digital Sight DSFi1 camera attached to a Nikon Eclipse 50i model microscope (Nikon Instruments Inc., Tokyo, Japan), utilizing NIS-Elements software (v. 4.50, Nikon Instruments). Microscope lamp intensities, exposure times, condenser aperture settings, video camera set-up and calibration, and use

of neutral density filters were kept constant for capturing all images of a particular immunostain.

Cortical thickness measurements, from the pial surface to the white matter, were made through the primary motor, frontal association, somatosensory, parieto-occipital, entorhinal, and primary visual cortices, as well as the cerebellum in Nissl-stained sections. The commissural thickness of the corpus callosum at sagittal level 5 was similarly measured. At least, 25 measurements were taken at regular intervals for each region from at least 2 animals per genotype per age.

For the immunohistochemical studies, data were collected from two animals of each genotype at each age. For threshold analysis, a set of nonoverlapping digital images (10 fields per region per animal for GFAP and GSB4; 1 hippocampal field from 15 animals per genotype across the time course for CLN5) were analyzed with the public domain ImageJ program (version 1.52P; NIH, Bethesda, MD, USA). Red bandwidth filters were applied for the DAB images, and the number of pixels with brightness levels above a set threshold was expressed as a percentage of the total pixel area. Threshold values for images of a particular immunostain at the same magnification were set so that positively stained structures at low reactivity were still selected, but not background staining in regions of high reactivity.

Ten digital images per region per animal were captured from unstained sections using a 450–490 nm excitation/510 nm emission filter set for the threshold analysis of storage body fluorescence.

2.5 | Statistical analyses

Statistical analyses were performed in GraphPad Prism (v 9.0.0, GraphPad Software, San Diego, CA, USA). Separate means (% area stained, cortical/commissural thickness) and standard errors of the mean were computed for each brain region for each animal and variable. Data were analyzed using two-way ANOVA (mixed-effects) followed by Dunnett's multiple comparisons test and multiple unpaired *t*-tests assuming unequal variances using a false discovery approach with a two-stage up method of Benjamini, Krieger, and Yekutieli with a $Q = 1\%$. For graph readability, statistical differences to control sheep determined by the false discovery rate-adjusted *p*-values are reported in the Supporting Information section.

3 | RESULTS

3.1 | Brain mass and gross atrophy

No differences were discernible in brain mass or macroscopic appearance between healthy control and affected sheep at birth. All brains grew rapidly until 4–6 months of age

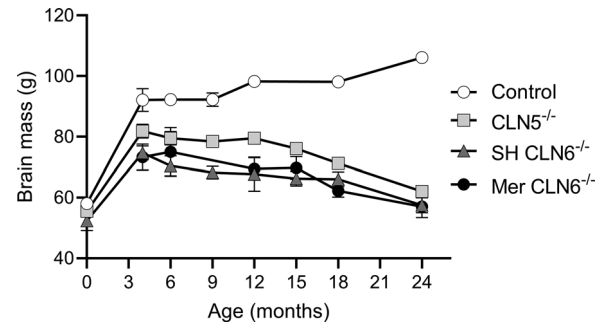


FIGURE 1 Mean brain mass changes (\pm SEM) in ovine CLN5 and CLN6 disease. Control brains grew to maturity at 24 months of age, whereas the brains of CLN5^{-/-}, South Hampshire CLN6^{-/-}, and Merino CLN6^{-/-} sheep were significantly lighter from 4 to 6 months of age ($p < .05$) and progressively atrophied. Numbers of brains collected for each genotype and age group varied from 2 to 18 (see Table S1).

(Figure 1, Table S1). Control brains continued to grow to reach mature weight by 24 months of age, whereas progressive brain atrophy began in the affected brains. By 24 months of age, the CLN5^{-/-} and CLN6^{-/-} (SH and Mer) brain masses were only 58% and 54%, respectively, that of the healthy control.

From 6 months of age, it was macroscopically apparent that these diseases affected different brain regions to different extents. There was similar progressive volume loss in the parietal and occipital lobes, medial and caudal to the suprasylvian sulcus, of both CLN5 and CLN6 affected brains, with concomitant dorsoventrally flattened, narrowed gyri, and widened sulci by 18–24 months (Figure 2). In contrast, the cerebellum and subcortical structures of all three affected models were remarkably preserved, even at end-stage disease (Figures 2 and 3).

3.2 | Regional atrophy

Consistent with previous SH CLN6^{-/-} findings (Kay et al., 2006; Oswald et al., 2005), the cytoarchitecture of the CLN5^{-/-} brain was normal in appearance at birth; however, laminar disruption occurred as early as 3 months of age in the primary visual and parieto-occipital cortices. This was accompanied by the progressive appearance of clusters of densely packed cellular aggregates at the layer I/II laminar boundary (Figure 3). These degenerative laminar changes spread from the primary visual and parieto-occipital cortices to the somatosensory cortex at 3 months (CLN5^{-/-}) and 6 months (SH CLN6^{-/-}) and were also present in the same three regions at the earliest time point examined for the Mer CLN6^{-/-} disease model (6 months). They reached the primary motor cortex by 9 (CLN5^{-/-} and Mer CLN6^{-/-}) to 12 months (SH CLN6^{-/-}), and the entire cortical mantle by 18 months for all three disease models.

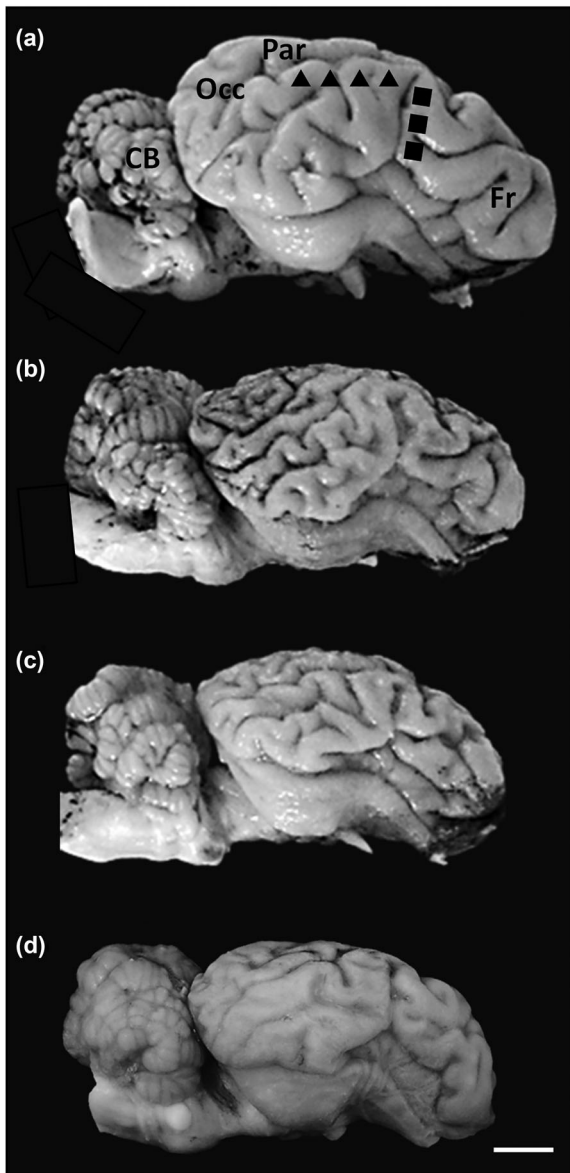


FIGURE 2 Lateral view of the control and affected sheep brain. Perfused brains from (a) a 19.2-month-old control sheep, (b) a 19.2-month-old CLN5^{-/-} sheep, (c) a 19.3-month-old SH CLN6^{-/-} sheep, and (d) a 19.4-month-old Mer CLN6^{-/-} sheep. There is marked atrophy of the diseased cerebral hemispheres and relative sparing of the cerebella. Brain weights were 99, 74.9, 60.8, and 61.0 g respectively. The cerebellum (CB), suprasylvian sulcus (▲), pseudosylvian sulcus (■), parietal (Par), occipital (Occ), and frontal (Fr) lobes are indicated. Scale bar represents 1 cm.

Cortical thickness measurements from Nissl-stained sagittal sections confirmed the similar progressive regionality of the neuronal loss in both disease forms (Figure 4, Table S2). A near-linear decline in cortical thickness in the primary visual, parieto-occipital, and somatosensory cortices began perinatally for all three disease models and reached statistical significance ($p \leq .05$) by 6–9 months of age. By end-stage disease at 18–24 months of age, thickness

measurements in all three affected sheep models ranged from 30% to 42% (parieto-occipital cortex), 34%–37% (primary visual cortex) to 39%–50% (somatosensory cortex) that of age-matched control brains.

The rate decline was initially slower in the frontal-association cortex, with atrophy in this region first seen in the CLN5^{-/-} brain before CLN6^{-/-} diseased brains, but affected frontal-association cortical thicknesses were reduced to 52%–63% of control sheep at termination. The entorhinal and primary motor cortices were also least affected early in disease and even experienced some growth in diseased sheep over the first 6–12 months of life before atrophy became established and by end-stage disease thickness measurements in these two regions were reduced to 44%–56% that of controls.

Pronounced thinning occurred earliest in the Mer CLN6^{-/-} brains for some cortical regions, particularly the entorhinal, primary motor, and parieto-occipital cortices, whereas atrophy was typically slowest in SH CLN6^{-/-} sheep. However, by 18–24 months of age, cortical atrophy was extensive and few large cortical neurons remained in any diseased sheep brain.

In contrast to the gross atrophy and neuronal loss of the cortex, the subcortical structures were remarkably preserved in all three disease models. There was no overt depletion of cells in the affected thalamic nuclei, colliculi, striatum, or cerebellum, and cerebellar thicknesses were not significantly different from controls throughout the disease course (Figure 4).

White matter tract abnormalities accompanied progressive atrophic changes in the affected cortical gray matter (Figure 5). The thickness of the corpus callosum in normal brains increased to plateau at $1326 \pm 161 \mu\text{m}$ ($n = 4$) by 18–24 months, whereas it remained relatively unchanged in all NCL affected sheep across postnatal development (CLN5^{-/-} $756 \pm 68 \mu\text{m}$ ($n = 10$); SH CLN6^{-/-} $725 \pm 58 \mu\text{m}$ ($n = 10$); Mer CLN6^{-/-} $737 \pm 113 \mu\text{m}$ ($n = 6$)).

3.3 | Neuroinflammation

Glial cell activation was assessed over disease progression by immunohistochemistry, using GFAP as an astrocytic marker and GSB4 lectin histochemistry to detect microglia.

Low-level GFAP reactivity was limited to quiescent protoplasmic astrocytes in lamina 1, adjacent to the pial surface, or distributed evenly within the gray matter laminae and white matter tracts in control brains at all ages (Figure 6a). In marked contrast, discrete foci of reactive hypertrophic astrocytes were present as early as birth in the CLN5^{-/-} and SH CLN6^{-/-} brain but were initially restricted to superficial laminae in the same cortical regions that first undergo neurodegeneration (e.g., the primary visual and parieto-occipital cortices). With age, these reactive astroglia spread to form a dense network throughout all cortical laminae in affected sheep (Figure 6a)

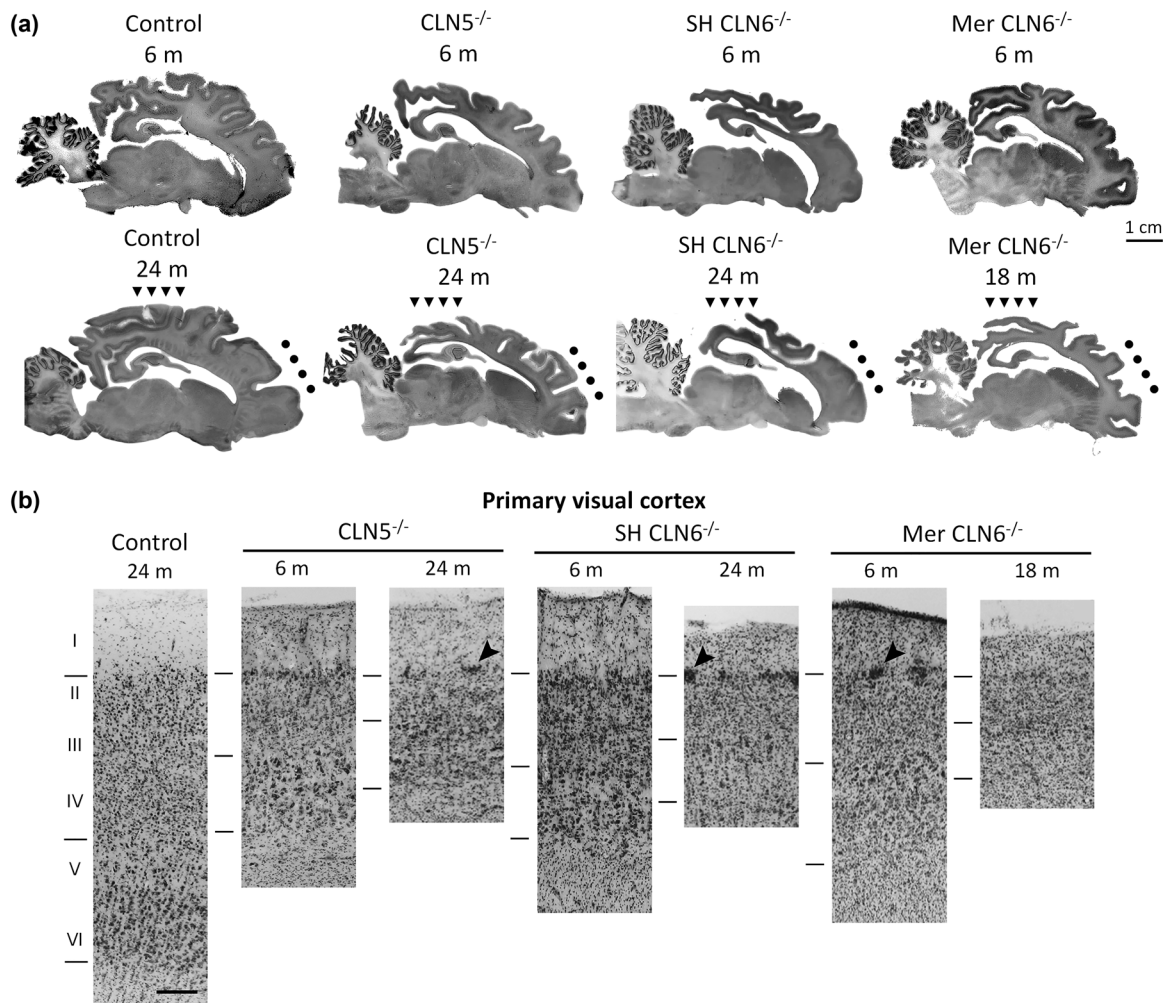


FIGURE 3 Marked cortical atrophy in ovine CLN5 and CLN6 disease. (a) Nissl-stained sagittal sections showing the gross atrophy of the cerebral cortex in affected sheep at 18–24 months, particularly in the primary visual cortex (▼). The vulnerability of the primary motor cortex (●) at end-stage disease is highlighted in the Mer CLN6^{-/-} sheep. In contrast, the cerebellum is relatively spared in all three disease models. (b) Microscopic comparison of the primary visual cortex in Nissl-stained sections. Pronounced atrophy and formation of cellular aggregates (arrowheads) began first and was more advanced, in the primary visual cortex for all three neuronal ceroid lipofuscinosis (NCL) affected sheep models. Upper lines mark the layer I/II boundary, the middle lines indicate layer IV, and the lower lines mark the layer VI/white matter boundary. Scale bar represents 200 μm .

and, to a lesser extent, subcortical regions. Affected Merino brain samples were not available for the early disease stages but showed a similar glial response to the other ovine models over the later disease course.

Quantitative threshold image analysis confirmed a parallel spatiotemporal spread of astrogliosis among the three disease models (Figure 6b, Table S3). There was significantly more GFAP immunoreactivity in the affected sheep cortices than age-matched control brain tissue ($p \leq .05$) at all ages assessed and the differences between control and affected subcortical structures also reached statistical significance by end-stage disease. In contrast, no astrocytic activation was found in the cerebellum of any of the ovine disease models; in fact, there was consistently less GFAP expression than in age-matched controls.

Neuroinflammatory GSB4 staining followed a similar pattern, being markedly increased in the cortical gray matter of both CLN5 and CLN6 affected sheep brains compared with controls. Initial clusters of activated microglia were detected in the superficial CLN5^{-/-} and SH CLN6^{-/-} neocortex at birth, and in Mer CLN6^{-/-} brains when first assessed at 6 months. These spread to deeper cortical laminae, particularly VI and the white/gray matter boundary, and increasing numbers of cells with amoeboid or brain macrophage-like morphology were observed across the brain with age (Figure 7a).

Thresholding quantification of GSB4 staining confirmed significant increases in activated microglia, first revealed in the primary visual and parieto-occipital cortices, and later in the primary motor cortex and occipital white matter of all

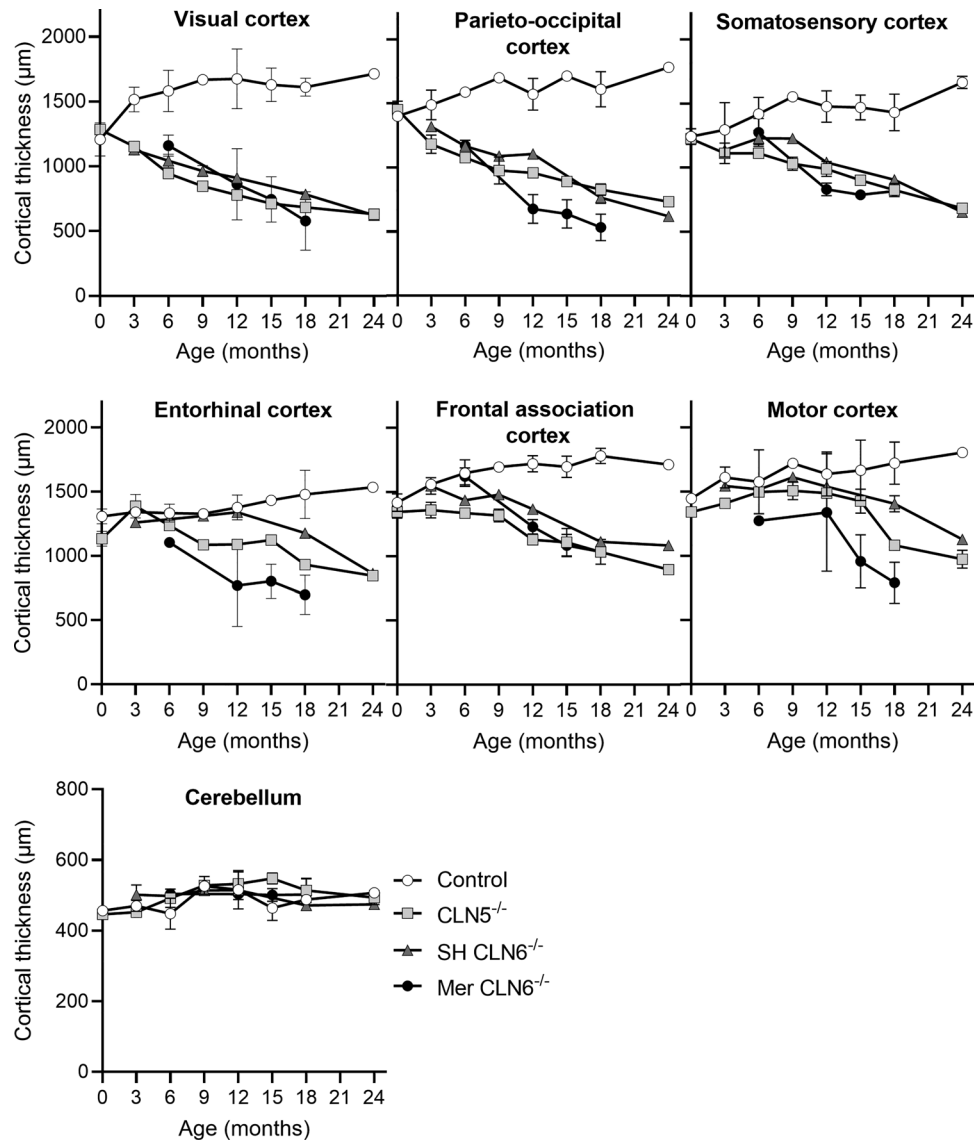


FIGURE 4 Progressive cortical atrophy in ovine CLN5 and CLN6 disease. Cortical thickness measurements revealed progressive thinning of the affected cortical mantle, but at variable rates in different regions. Atrophy was first and most evident in the primary visual, parieto-occipital, and somatosensory cortices, before spreading to the primary motor cortex by 12–18 months of age. Pronounced thinning occurred earliest in the Mer CLN6^{-/-} sheep brain for at least three cortical regions. For all time points, $n \geq 2$ animals/group, however, 25 individual measurements were taken per animal. Significant thickness differences to control sheep are reported in Table S2.

three disease models ($p \leq .05$) (Figure 7b, Table S4). A trend toward greater activation was observed in most regions of the CLN5^{-/-} brain but this was not statistically confirmed.

The granular cell layer of the cerebellum stained heavily with the GSB4 lectin in both control and affected sheep brains but amoeboid microglial cell infiltration of the cerebellar white matter was not noted in the disease models until 18–24 months of age. Microgliosis was also grossly apparent in other subcortical structures at end-stage disease, particularly the lateral geniculate nucleus, hippocampus, and thalamic nuclei but this was much delayed, and minor compared with that in the affected cortices.

3.4 | Lysosomal storage

Progressive lysosomal storage was quantified in the sheep brain by fluorescent microscopy and threshold analysis (Figure 8, Table S5). In the initial disease stages (≤ 6 months of age), small punctate fluorescent aggregates were confined to cells with characteristic neuronal morphology in all laminae of the cerebral cortex, the subcortical nuclei, pyramidal cells of the hippocampus, and Purkinje cells in the cerebellum. They later appeared in nonneuronal cells as the disease progressed.

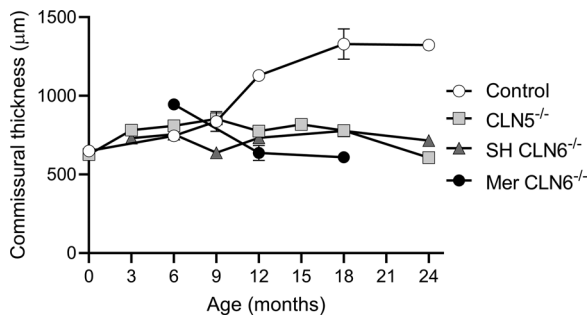


FIGURE 5 White matter changes in ovine CLN5 and CLN6 disease. The commissural white matter tract thickened in control animals between birth and 24 months of age but was obviously thinner in affected sheep from 12 months of age, maintaining a constant thickness over the same time period. For all time points, $n = 2$ animals/group.

Lysosomal accumulation in the three ovine NCL forms was comparable (Figure 8a), with earlier and greater storage levels in the primary visual cortex than the parieto-occipital and primary motor cortices (Figure 8b). Even slower accumulation was noted in subcortical regions, yet fluorescent storage levels in all regions examined in the affected brains followed a near-linear increase from birth in all regions analyzed and, except for the occipital white matter, were statistically different ($p \leq .05$) to controls from 6 months of age. Storage was universal throughout all affected gray and white matter regions at end-stage disease.

3.5 | Clinical-pathological correlation

The neuropathological changes identified in this study were correlated with previously published clinical findings for the three sheep disease models (Cook et al., 2002; Cronin et al., 2016; Jolly et al., 1989, 2002; Mayhew et al., 1985; Mitchell et al., 2018; Russell et al., 2018, 2021) (Table 1).

4 | DISCUSSION

Despite the very different gene products and subcellular localizations underlying these three ovine diseases, their pathogenic cascades were remarkably comparable. The greatest variation was that neurodegenerative thinning occurred earlier, and at a greater rate, in the Mer CLN6^{-/-} brain for many cortical regions, particularly the entorhinal, primary motor, and parieto-occipital cortices, whereas atrophy was typically slowest in SH CLN6^{-/-} sheep. Yet at 24 months of age, average brain masses were very similar for the three disease models, suggesting that despite these subtle differences in the pathogenic cascade, the pathological endpoint was the same. Importantly too, this study corroborated the

previous published SH CLN6 neuropathological findings (Oswald et al., 2005) and extended those findings to show very delayed, albeit significant, atrophy in the CLN6 motor cortex at terminal disease.

At birth, CLN5^{-/-} and SH CLN6^{-/-} sheep already have punctate lysosomal storage body accumulation in neuronal cells, which demonstrated a near-linear increase across the brain with age. Despite the near-ubiquity of the lysosomal storage, the development of neuroinflammation and neurodegeneration was more regionally dependent. Discrete foci of hypertrophic astrocytes noted at birth in the CLN5 affected (this study) and SH CLN6 affected sheep brains (Kay et al., 2006; Oswald et al., 2005) initially localized to the more superficial cortical laminae in the first areas to undergo neurodegeneration (the primary visual and parieto-occipital cortices). With increasing age, reactive glia spread to form a dense meshwork across the cortex of all three disease models, in a regionally specific manner preceding and accurately predicting the subsequent neuronal loss, and subcortical regions become involved. Neurodegeneration in affected sheep, evident by cortical thinning measurements, began before clinical symptomatology, and by end-stage disease at 18–24 months, the entire cortical mantle was atrophied and consisted of a dense network of reactive astrocytes and brain macrophages with few neurons remaining.

In comparison, the subcortical structures and cerebellum were relatively preserved in all three ovine disease models. End-stage magnetic resonance imaging (MRI) studies in CLN5^{-/-} and CLN6^{-/-} affected sheep corroborate this structural finding (Amorim et al., 2015; Beganovic et al., 2012; Murray et al., 2022; Sawiak et al., 2015). However, this does contrast with the characteristic cerebellar pathology seen in human CLN5 and CLN6. Cerebella from human CLN6 patients may be normal or show some atrophy (Cannelli et al., 2009; Peña et al., 2001), but it has been reported that the cerebellum in human CLN5 cases can be severely atrophied, with an almost complete depletion of cerebellar granule and Purkinje cells observed in post mortem tissue (Goebel et al., 1999; Haltia, 2003; Tyynelä et al., 1997). Brain imaging of human CLN5 patients reveals the same moderate-to-severe cortical atrophy seen in CLN5 animal models, but marked atrophy of the human cerebellum is one of the most striking abnormalities (Autti et al., 1992; Azad et al., 2020; Bessa et al., 2006; Lauronen et al., 2002; Mancini et al., 2015; Simonati et al., 2017).

This is not the case for most animal CLN5 and CLN6 NCLs. Naturally occurring CLN6 (*nclf*) mice exhibit progressive retinal atrophy, neurodegeneration, and premature death (Bronson et al., 1993; Mirza et al., 2013; Morgan et al., 2013), but the CLN5 exon 3 knockout mouse model lacks the severe brain (cortical and cerebellar) atrophy characteristic of the human disease (Kopra et al., 2004). Only mild cerebellar atrophy was reported for the Devon cattle CLN5

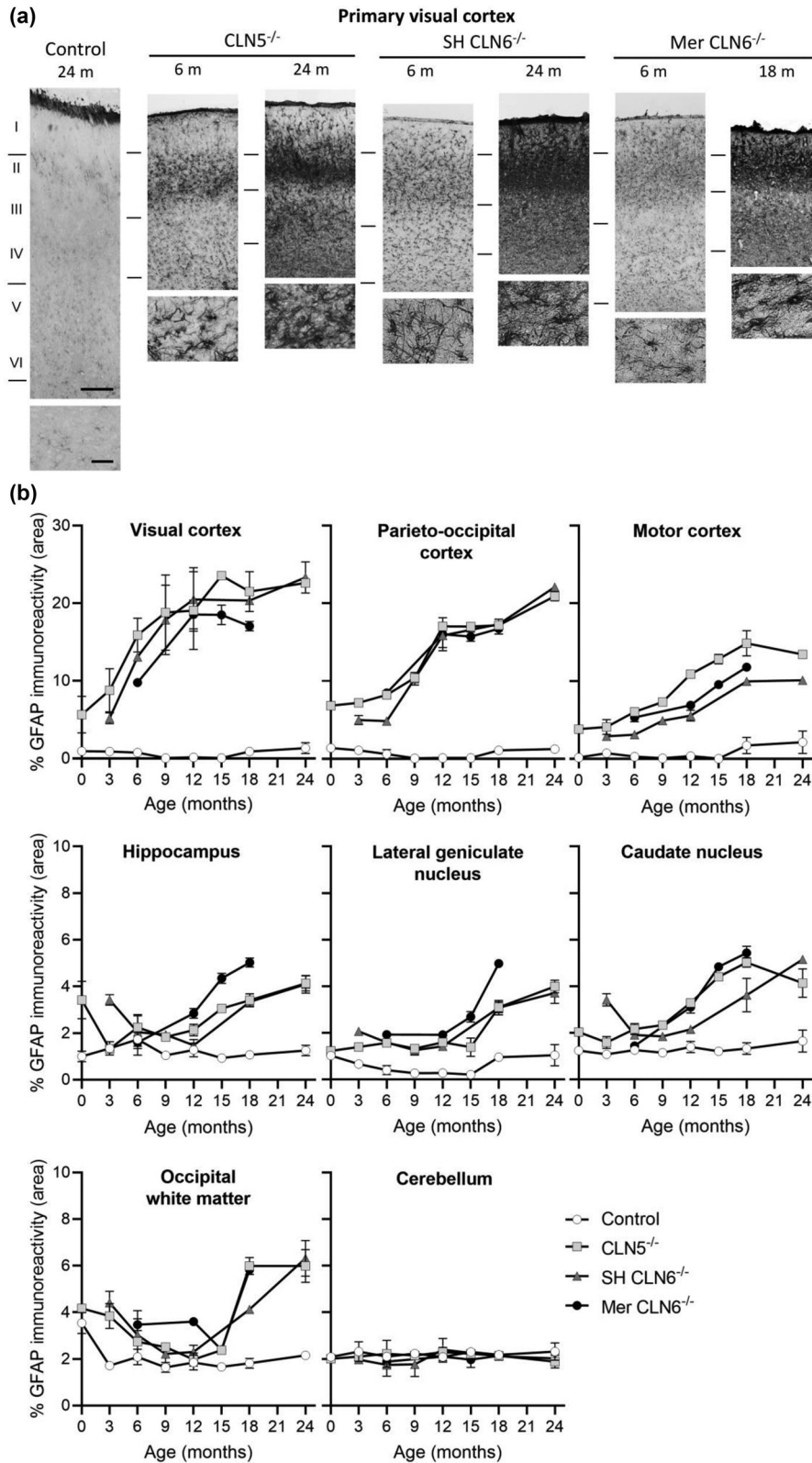


FIGURE 6 Progressive astrocytosis in ovine CLN5 and CLN6 disease. (a) Glial fibrillary acidic protein (GFAP) immunohistochemistry of the primary visual cortex revealed astrocytic spread from specific foci in the upper cortical layers to a dense glial network across all cortical layers with disease progression. Scale bars represent 200 μm (upper) and 50 μm (lower). (b) Threshold GFAP image analyses confirmed widespread and progressive astrocytic activation in the affected sheep brain of all three disease models. Immunoreactivity was most pronounced in the primary visual cortex, spreading with time to other cortical regions with a much-delayed response in subcortical structures. Significant immunoreactivity differences to control sheep are reported in Table S3.

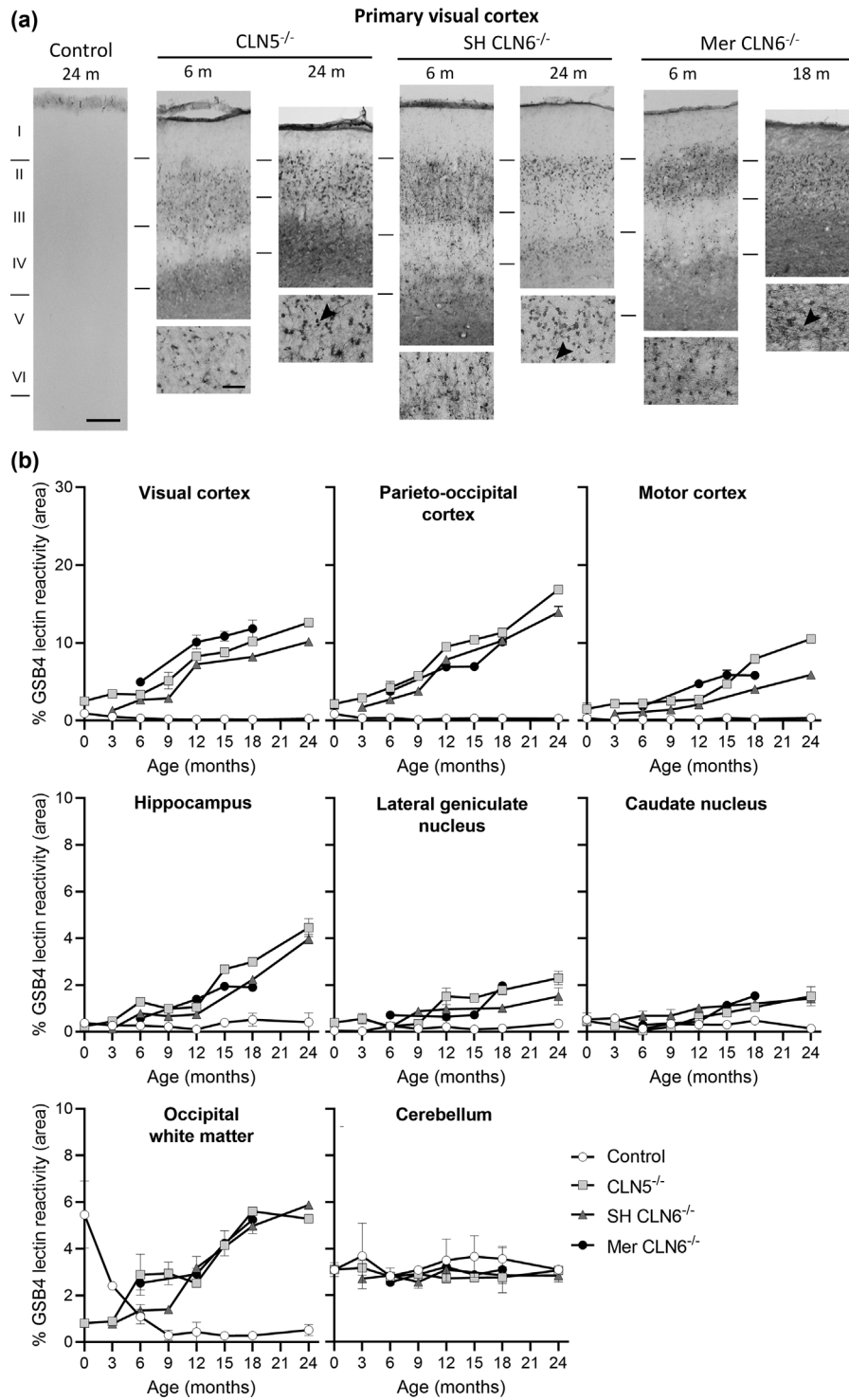


FIGURE 7 Progressive microgliosis in ovine CLN5 and CLN6 disease. (a) GSB4 lectin histochemistry of the primary visual cortex revealed hypertrophic microglial activation from specific foci in the upper cortical layers to encompass all cortical layers with disease progression. Brain macrophages were noted in the affected brains at higher magnification (arrowheads, lower boxes). Scale bars represent 200 μm (upper) and 50 μm (lower). (b) Threshold GSB4 image analyses confirmed widespread and progressive microglial activation in the affected sheep brain of all three disease models. Reactivity was most pronounced in the primary visual cortex, spreading with time to other cortical regions with a much-delayed response in subcortical structures. Significant lectin reactivity differences to control sheep are reported in Table S4.

TABLE 1 Summary overview of pathological and phenotypic traits in the three sheep models.

Age	Mean brain weight (g) ^a			Clinical phenotype (published literature)	Neuropathological changes (current study)
	CLN5	CLN6 SH	CLN6 Mer		
Birth	56 (96%)	52 (90%)	N.d.	Normal	Sparse lysosomal storage in neuronal cells. Neuroinflammatory foci in upper laminae of V1 and POC <i>Similar changes previously documented for SH CLN6^{-/-} Neuropathology not examined in Mer CLN6^{-/-}</i>
3–4 months	82 (89%)	75 (81%)	73 (80%)	As birth	Similar to birth <i>Neuropathology not examined in Mer CLN6^{-/-}</i>
6 months	80 (86%)	70 (76%)	75 (81%)	Low head carriage, propensity to baulk, crouch, and stumble	Widespread storage, mainly in neuronal cells. Neuroinflammation in upper laminae spread across the cortical mantle. Obvious neuronal loss and atrophy in V1, S1, and POC
9 months	78 (85%)	68 (74%)	N.d.	Visual deficits, star-gazing, decreased or lost menace response, depressed PLR and dazzle reflexes, reduced herding. Reduced ERG in CLN5 ^{-/-} and SH CLN6 ^{-/-} <i>ERG not examined in Mer CLN6^{-/-}</i>	Obvious neuronal loss and atrophy in most cortical regions, except M1 <i>Neuropathology not examined in Mer CLN6^{-/-}</i>
12 months	78 (81%)	68 (69%)	69 (71%)	Onset of motor, cognitive, and proprioceptive deficits, including ataxia, wide stance, reduced mentation, and stereotypical behavior	Widespread storage in neuronal and nonneuronal cells. Neuroinflammation spread to deeper laminae across the cortex. Obvious neuronal loss and atrophy in all cortical regions, except M1
15 months	76 (78%)	66 (68%)	70 (71%)	Progressive disease, compulsive circling, ± inducible tetanic seizures. Extinguished ERG in SH CLN6 ^{-/-} <i>ERG not examined in Mer CLN6^{-/-}</i>	Widespread storage, neuronal loss, and neuroinflammation across the entire cortex, much less in subcortex <i>Neuropathology not examined in SH or Mer CLN6^{-/-}</i>
18 months	71 (73%)	66 (67%)	62 (63%)	Progressive disease ± spontaneous seizures. Extinguished ERG in CLN5 ^{-/-} <i>ERG not examined in Mer CLN6^{-/-}</i>	Storage mainly in nonneuronal cells and brain macrophages, dense meshwork of neuroinflammation throughout the brain. Dramatic neuronal cell loss. Few large cortical neurons remain in Mer CLN6 ^{-/-}
>24 months	62 (58%)	58 (54%)	57 (54%)	Terminal Severely reduced or extinguished ERG in Mer CLN6 ^{-/-}	Few large cortical neurons remain in CLN5 ^{-/-} and SH CLN6 ^{-/-} <i>Neuropathology not examined in Mer CLN6^{-/-}</i>

^aPercentage represents comparative mean brain weight of healthy control sheep.

Abbreviations: ERG, electroretinography; m, months; M1, primary motor cortex; Mer, Merino; N.d., No data available; PLR, pupillary light reflex; POC, parieto-occipital cortex; S1, somatosensory cortex; SH, South Hampshire; V1, primary visual cortex.

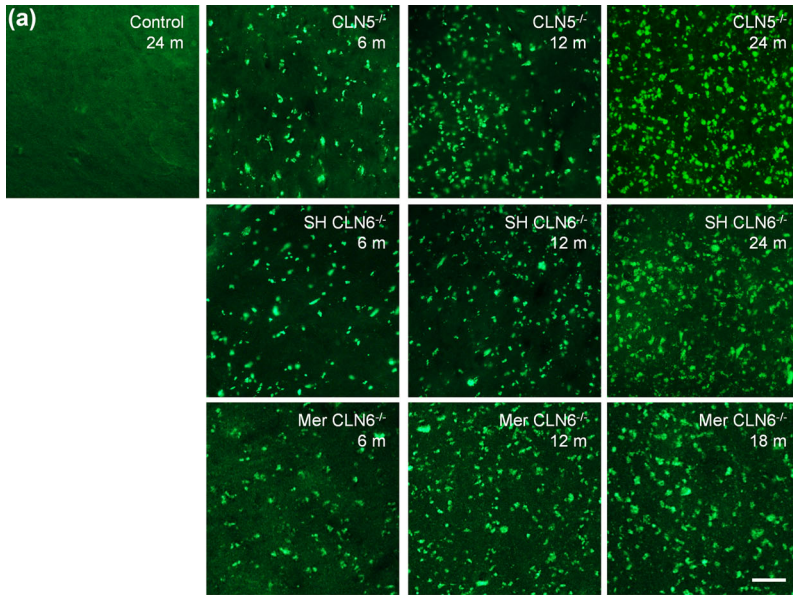
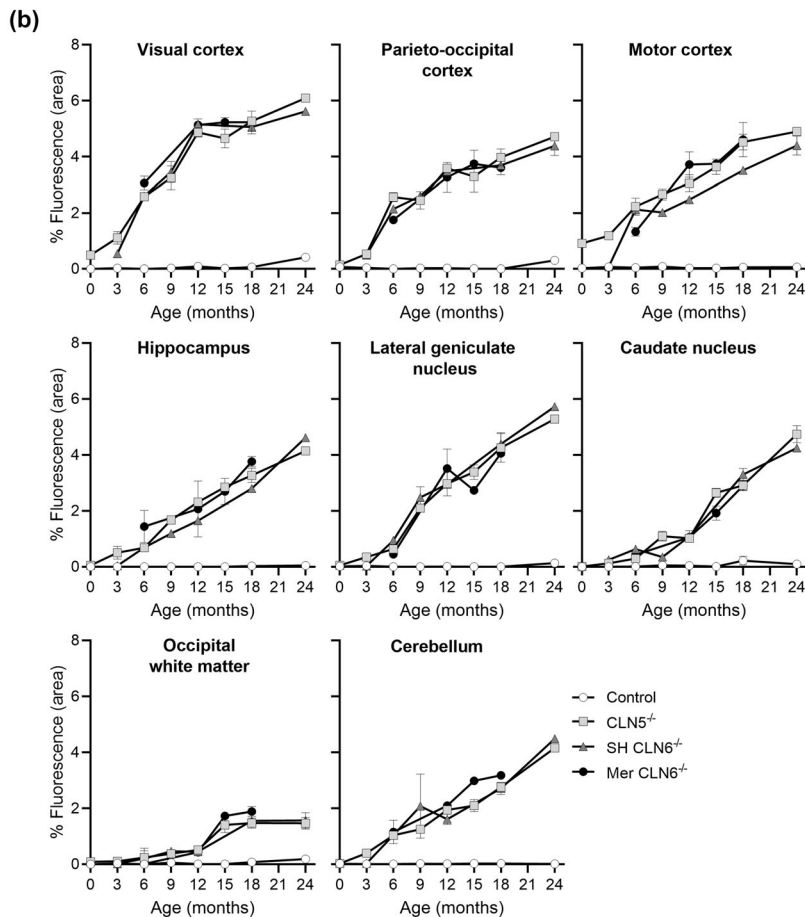


FIGURE 8 Progressive storage body accumulation in ovine CLN5 and CLN6 disease. (a) Fluorescent microscopy revealed lysosomal storage accumulation in the parieto-occipital cortex over disease progression. Scale bar represents 50 μm . (b) Threshold analyses confirmed widespread and progressive fluorescent storage body accumulation across the affected sheep brain for all three disease models. Significant fluorescence differences to control sheep are reported in Table S5.



model (Jolly et al., 1992), and dilated cerebellar sulci without gross degeneration are seen in MRI or computed tomography studies of canine Border collie, Australian cattle dog, and Golden retriever CLN5 (Koie et al., 2004; Kolicheski et al., 2016; Meiman et al., 2022; Mizukami et al., 2012). The reason why cerebellar pathology, aside from lysosomal storage and the late-stage white matter microgliosis detected here in

sheep, does not often manifest in animal NCLs is unclear. It may be that the degenerative effects of the disease seen in the cerebral cortex are simply delayed in the cerebellum, and affected animals do not live long enough to exhibit extra-cortical pathology. Life expectancy in the three Australasian NCL sheep models is typically limited to 18–24 months of age. However, this is a humane terminal endpoint, specified

by when the sheep's quality of life is dramatically reduced, or they can no longer live independently. This is a very different proposition to the life expectancy of affected children, who may experience long periods of palliative and end-of-life care. It is not known if later cerebella changes would manifest in sheep or other affected animals if they were similarly treated.

These neuropathology studies are in line with prior clinical studies which also reported remarkably similar disease progression in the three Australasian ovine NCL models (Cook et al., 2002; Cronin et al., 2016; Jolly et al., 1989, 2002; Mayhew et al., 1985; Mitchell et al., 2018; Russell et al., 2018, 2021) (Table 1). The homochronic clinicopathological development between diseases caused by different mutations affecting dissimilar gene products strongly indicates some as yet undiscovered connection between them. That they all result in the abnormal accumulation of the c subunit of mitochondrial ATP synthase (Palmer, 2015) reinforces that conclusion. Furthermore, the human CLN5 and CLN6 diseases are also akin to those in these sheep. Human CLN5 mutations generally cause NCL with onset in late infancy, the most common presenting symptom being motor dysfunction at 4–7 years of age, followed by progressive visual decline, seizures, dementia, and premature death between the ages of 14 and 36 years (Nita et al., 2016; Simonati et al., 2017). The majority of CLN6 patients experience early visual failure between 3 and 5 years of age—an analogs age of onset—but deterioration is more rapid and most children die before their early teens (Nita et al., 2016).

Whether the greater range of disease development in humans is caused by the differences in mutations or is a result of different genetic backgrounds has been explored but is uncertain (Gardner & Mole, 2021). The tight homochronic disease presentations in CLN5 and CLN6 sheep may be due to their similar narrow genetic backgrounds, being that all Australasian sheep originally arose from flocks imported into Australia in the 19th century. An interesting adjunct to this study will be to compare the neuropathology in the recently developed Texel-cross CLN1 sheep to these ovine models. Unlike the naturally occurring Australasian disease models, the CLN1^{-/-} sheep were generated through CRISPR-Cas9 gene editing (OMIA 001504-9940) (Eaton et al., 2019). They exhibit a similar clinical disease progression to the CLN5^{-/-} and CLN6^{-/-} sheep, with loss of vision, behavioral, and motor deficits, but were humanely euthanized at an earlier terminal endpoint of 17 ± 1 months. At this age, brain mass was 30% of normal, a value comparable to CLN5^{-/-} and CLN6^{-/-} sheep at a similar age, and again the atrophy was predominantly cortical (Eaton et al., 2019).

The cortical thickness measurements used in this study allowed comparison of the gross regional integrity across the brain over time but may not be the most sensitive measure of overall atrophy. Of note, cortical thickness can be influenced

by nonneuronal (glial) composition, neuropil volume, including myelination, spine density, and dendritic arborization, and neuronal soma size, so it will be necessary to perform further neuronal counts in the three disease models to establish the true extent of neuronal cell loss in the early postnatal stages and categorically distinguish the onset of neurodegeneration from gliosis and developmental deficits.

Finally, an important question for therapy is when does the pathogenic cascade become fatally damaging to neurons? Correlation of the neuropathological findings from this study with published clinical data on ovine CLN5 and CLN6 disease has identified three different ages in affected sheep in which to explore the window for best therapeutic intervention. As with all lysosomal storage diseases, the earlier the intervention, the greater the chance of maximizing therapeutic benefit. As such, 3 months of age represents a presymptomatic disease stage. Although the brain has almost reached peak weight, there is established gliosis, mild neuronal loss, and sparse lysosomal storage but this is a common age to wean lambs, and diseased sheep do not exhibit clinical signs at this age (Mitchell et al., 2018; Tammen et al., 2001; Westlake et al., 1995). Given that most human cases of Batten disease only become apparent on diagnosis following the development of disease symptoms, CLN5^{-/-} and CLN6^{-/-} sheep at 6 months of age represent an early-symptomatic disease stage. At this age, affected sheep demonstrate mild movement dysfunction and early visual loss and gross cortical atrophy and neurodegeneration is overt. Finally, 9 months of age represents a later symptomatic disease stage, with sufficient neurons surviving to potentially afford therapeutic benefit. At this age, affected sheep demonstrate clear phenotypic deficits, particularly related to visual loss, and the affected brain has reduced to ~74%–85% the weight of a normal brain. Assessing the efficacy of treatments delivered at each of these disease stages in sheep should provide good translational preclinical data for human studies.

In conclusion, this study presents a comprehensive investigation of neuropathological changes in three sheep models of NCL. Insight was provided into the optimal age/disease stage for therapeutic intervention and the study identified terminal efficacy endpoints, including brain weight, quantification of neurodegeneration, neuroinflammation, and lysosomal storage burden. These will be used with our published longitudinal in vivo safety and efficacy endpoints, such as survival, body weight, clinical scoring, maze testing, electroretinography, and neuroimaging (Mitchell et al., 2018; Murray et al., 2022; Russell et al., 2018, 2021) in current and future gene therapy studies utilizing these sheep models of NCL.

AUTHOR CONTRIBUTIONS

All authors had full access to all the data in the study and take responsibility for the integrity of the data and the accuracy

of the data analysis. Conceptualization: Nadia L. Mitchell, Katharina N. Russell. Methodology: Nadia L. Mitchell, Katharina N. Russell. Investigation: Nadia L. Mitchell, Katharina N. Russell. Formal analysis: Nadia L. Mitchell, Katharina N. Russell. Resources: Imke Tammen, David N. Palmer. Writing—original draft: Nadia L. Mitchell, Katharina N. Russell. Writing—review and editing: Nadia L. Mitchell, Katharina N. Russell, Graham K. Barrell, Imke Tammen, David N. Palmer. Supervision: Graham K. Barrell, Imke Tammen, David N. Palmer. Funding acquisition: Imke Tammen, David N. Palmer.

ACKNOWLEDGMENTS

Our thanks to the staff of the Johnstone Memorial Laboratory and Ashley Dene research farm in New Zealand and Mayfarm, University of Sydney in Australia for animal care and provision. This research was funded by the Batten Disease Support and Research Association (to DNP and IT). N.L.M. was supported by a John W. and Carrie McLean Trust PhD scholarship, and K.N.R. was supported by a MARS Bioimaging Ltd PhD stipend.

Open access publishing facilitated by Lincoln University, as part of the Wiley - Lincoln University agreement via the Council of Australian University Librarians.

CONFLICT OF INTEREST STATEMENT

The authors declare no conflict of interests.

DATA AVAILABILITY STATEMENT

The data that support the findings of this study are available within the article and its supporting information files.

ORCID

Nadia L. Mitchell  <https://orcid.org/0000-0003-4801-2804>

Graham K. Barrell  <https://orcid.org/0000-0001-7644-6816>

Imke Tammen  <https://orcid.org/0000-0002-5520-6597>

David N. Palmer  <https://orcid.org/0000-0002-9703-5351>

REFERENCES

- Amorim, I. S., Mitchell, N. L., Palmer, D. N., Sawiak, S. J., Mason, R., Wishart, T. M., & Gillingwater, T. H. (2015). Molecular neuropathology of the synapse in sheep with CLN5 Batten disease. *Brain and Behavior*, 5(11), e00401. <https://doi.org/10.1002/brb3.401>
- Autti, T., Raininko, R., Launes, J., Nuutila, A., & Santavuori, P. (1992). Jansky-Bielschowsky variant disease: CT, MRI, and SPECT findings. *Pediatric Neurology*, 8(2), 121–126. [https://doi.org/10.1016/0887-8994\(92\)90032-T](https://doi.org/10.1016/0887-8994(92)90032-T)
- Azad, B., Efthymiou, S., Sultan, T., Scala, M., Alvi, J. R., Neuray, C., Dominik, N., Gul, A., & Houlden, H. (2020). Novel likely disease-causing CLN5 variants identified in Pakistani patients with neuronal ceroid lipofuscinosis. *Journal of the Neurological Sciences*, 414, 116826. <https://doi.org/10.1016/j.jns.2020.116826>
- Bajaj, L., Sharma, J., di Ronza, A., Zhang, P., Eblimit, A., Pal, R., Roman, D., Collette, J. R., Booth, C., Chang, K. T., Sifers, R. N., Jung, S. Y., Weimer, J. M., Chen, R., Schekman, R. W., & Sardiello, M. (2020). A CLN6-CLN8 complex recruits lysosomal enzymes at the ER for Golgi transfer. *Journal of Clinical Investigation*, 140(8), 4118–4132. <https://doi.org/10.1172/JCI130955>
- Beganovic, D. F., Sutton, A., Cronin, G. M., Hughes, K., Zaki, S., Thomson, P., & Tammen, I. (2012). Behavioural studies and magnetic resonance imaging in the Merino sheep NCL model. In 13th International Conference on Neuronal Ceroid Lipofuscinoses (Batten Disease) London, UK, P18.
- Bessa, C., Teixeira, C. A. F., Mangas, M., Dias, A., Sá Miranda, M. C., Guimaraes, A., Ferreira, J. C., Canas, N., Cabral, P., & Ribeiro, M. G. (2006). Two novel CLN5 mutations in a Portuguese patient with vLINCL: Insights into molecular mechanisms of CLN5 deficiency. *Molecular Genetics and Metabolism*, 89(3), 245–253. <https://doi.org/10.1016/j.ymgme.2006.04.010>
- Bronson, R. T., Lake, B. D., Cook, S., Taylor, S., & Davisson, M. T. (1993). Motor neuron degeneration of mice is a model of neuronal ceroid lipofuscinosis (Batten's disease). *Annals of Neurology*, 33(4), 381–385. <https://doi.org/10.1002/ana.410330408>
- Butz, E. S., Chandrachud, U., Mole, S. E., & Cotman, S. L. (2020). Moving towards a new era of genomics in the neuronal ceroid lipofuscinoses. *Biochimica et Biophysica Acta—Molecular Basis of Disease*, 1866(9), 165571. <https://doi.org/10.1016/j.bbadis.2019.165571>
- Cannelli, N., Garavaglia, B., Simonati, A., Aiello, C., Barzaghi, C., Pezzini, F., Cilio, M. R., Biancheri, R., Morbin, M., Dalla Bernardina, B., Granata, T., Tessa, A., Invernizzi, F., Pessagno, A., Boldrini, R., Zibordi, F., Grazian, L., Claps, D., Carrozzo, R., ... Santorelli, F. M. (2009). Variant late infantile ceroid lipofuscinoses associated with novel mutations in CLN6. *Biochemical and Biophysical Research Communications*, 379(4), 892–897. <https://doi.org/10.1016/j.bbrc.2008.12.159>
- Cook, R. W., Jolly, R. D., Palmer, D. N., Tammen, I., Broom, M. F., & McKinnon, R. (2002). Neuronal ceroid lipofuscinosis in Merino sheep. *Australian Veterinary Journal*, 80(5), 292–297. <https://doi.org/10.1111/j.1751-0813.2002.tb10847.x>
- Cronin, G. M., Beganovic, D. F., Sutton, A. L., Palmer, D., Thomson, P. C., & Tammen, I. (2016). Manifestation of neuronal ceroid lipofuscinosis in Australian Merino sheep: Observations on altered behaviour and growth. *Applied Animal Behaviour Science*, 175, 32–40. <https://doi.org/10.1016/j.applanim.2015.11.012>
- Eaton, S. L., Proudfoot, C., Lilloco, S. G., Skehel, P., Kline, R. A., Hamer, K., Rzechorzek, N. M., Clutton, E., Gregson, R., King, T., O'Neill, C. A., Cooper, J. D., Thompson, G., Whitelaw, C. B., & Wishart, T. M. (2019). CRISPR/Cas9 mediated generation of an ovine model for infantile neuronal ceroid lipofuscinosis (CLN1 disease). *Scientific Reports*, 9(1), 9891. <https://doi.org/10.1038/s41598-019-45859-9>
- Eaton, S. L., & Wishart, T. M. (2017). Bridging the gap: Large animal models in neurodegenerative research. *Mammalian Genome*, 28, 324–337. <https://doi.org/10.1007/s00335-017-9687-6>
- Frugier, T., Mitchell, N. L., Tammen, I., Houweling, P. J., Arthur, D. G., Kay, G. W., van Diggelen, O. P., Jolly, R. D., & Palmer, D. N. (2008). A new large animal model of CLN5 neuronal ceroid lipofuscinosis in Borderdale sheep is caused by a nucleotide substitution at a consensus splice site (c.571 + 1G >A) leading to excision of exon 3. *Neurobiology of Disease*, 29(2), 306–315. <https://doi.org/10.1016/j.nbd.2007.09.006>

- Gardner, E., & Mole, S. E. (2021). The genetic basis of phenotypic heterogeneity in the neuronal ceroid lipofuscinoses. *Frontiers in Neurology*, 12(October), 754045. <https://doi.org/10.3389/fneur.2021.754045>
- Goebel, H. H., Schochet, S. S., Jaynes, M., Brück, W., Kohlschütter, A., & Hentati, F. (1999). Progress in neuropathology of the neuronal ceroid lipofuscinoses. *Molecular Genetics and Metabolism*, 66(4), 367–372. <https://doi.org/10.1006/mgme.1999.2808>
- Haltia, M. (2003). The neuronal ceroid-lipofuscinoses. *Journal of Neuropathology and Experimental Neurology*, 62(1), 1–13. <https://doi.org/10.1093/jnen/62.1.1>
- Heine, C., Koch, B., Storch, S., Kohlschütter, A., Palmer, D. N., & Braulke, T. (2004). Defective endoplasmic reticulum-resident membrane protein CLN6 affects lysosomal degradation of endocytosed arylsulfatase A. *The Journal of Biological Chemistry*, 279(21), 22347–22352. <https://doi.org/10.1074/jbc.M400643200>
- Huber, R., & Mathavarajah, S. (2018). CLN5 is secreted and functions as a glycoside hydrolase in *Dictyostelium*. *Cellular Signalling*, 42, 236–248. <https://doi.org/10.1016/j.cellsig.2017.11.001>
- Jolly, R. D., Arthur, D. G., Kay, G. W., & Palmer, D. N. (2002). Neuronal ceroid-lipofuscinosis in Borderdale sheep. *New Zealand Veterinary Journal*, 50(5), 199–202. <https://doi.org/10.1080/00480169.2002.36311>
- Jolly, R. D., Gibson, A. J., Healy, P. J., Slack, P. M., & Birtles, M. J. (1992). Bovine ceroid-lipofuscinosis: Pathology of blindness. *New Zealand Veterinary Journal*, 40(3), 107–111. <https://doi.org/10.1080/00480169.1992.35711>
- Jolly, R. D., Shimada, A., Dopfmer, I., Slack, P. M., & Palmer, D. N. (1989). Ceroid-lipofuscinosis (Batten's disease): Pathogenesis and sequential neuropathological changes in the ovine model. *Neuropathology and Applied Neurobiology*, 15(4), 371–383. <https://doi.org/10.1111/j.1365-2990.1989.tb01236.x>
- Kay, G. W., Palmer, D. N., Rezaie, P., & Cooper, J. D. (2006). Activation of non-neuronal cells within the prenatal developing brain of sheep with neuronal ceroid lipofuscinosis. *Brain Pathology*, 16(2), 110–116. <https://doi.org/10.1111/j.1750-3639.2006.00002.x>
- Kohlschütter, A., Schulz, A., Bartsch, U., & Storch, S. (2019). Current and emerging treatment strategies for neuronal ceroid lipofuscinoses. *CNS Drugs*, 33(4), 315–325. <https://doi.org/10.1007/s40263-019-00620-8>
- Koie, H., Shibuya, H., Sato, T., Sato, A., Nawa, K., Nawa, Y., Kitagawa, M., Sakai, M., Takahashi, T., Yamaya, Y., Yamato, O., Watari, T., & Tokuriki, M. (2004). Magnetic resonance imaging of neuronal ceroid lipofuscinosis in a Border Collie. *The Journal of Veterinary Medical Science*, 66(11), 1453–1456. <https://doi.org/10.1292/jvms.66.1453>
- Kolicheski, A., Johnson, G. S., O'Brien, D. P., Mhlanga-Mutangadura, T., Gilliam, D., Guo, J., Anderson-Sieg, T. D., Schnabel, R. D., Taylor, J. F., Lebowitz, A., Swanson, B., Hicks, D., Niman, Z. E., Wininger, F. A., Carpentier, M. C., & Katz, M. L. (2016). Australian cattle dogs with neuronal ceroid lipofuscinosis are homozygous for a CLN5 nonsense mutation previously identified in Border Collies. *Journal of Veterinary Internal Medicine*, 30(4), 1149–1158. <https://doi.org/10.1111/jvim.13971>
- Kopra, O., Vesa, J., von Schantz, C., Manninen, T., Minye, H., Fabritius, A. L., Rapola, J., van Diggelen, O. P., Saarela, J., Jalanko, A., & Peltonen, L. (2004). A mouse model for Finnish variant late infantile neuronal ceroid lipofuscinosis, CLN5, reveals neuropathology associated with early aging. *Human Molecular Genetics*, 13(23), 2893–2906. <https://doi.org/10.1093/hmg/ddh312>
- Lauronen, L., Huttunen, J., Kirveskari, E., Wikström, H., Sainio, K., Autti, T., & Santavuori, P. (2002). Enlarged SI and SII somatosensory evoked responses in the CLN5 form of neuronal ceroid lipofuscinosis. *Clinical Neurophysiology*, 113(9), 1491–1500. [https://doi.org/10.1016/S1388-2457\(02\)00200-6](https://doi.org/10.1016/S1388-2457(02)00200-6)
- Liu, W., Kleine Holthaus, S.-M., Herranz-Martin, S., Aristorena, M., Mole, S. E., Smith, A. J., Ali, R. R., & Rahim, A. A. (2020). Experimental gene therapies for the NCLs. *Biochimica et Biophysica Acta—Molecular Basis of Disease*, 1866(9), 165772. <https://doi.org/10.1016/j.bbadis.2020.165772>
- Luebben, A. V., Bender, D., Becker, S., Crowther, L. M., Erven, I., Hofmann, K., Söding, J., Klemp, H., Bellotti, C., Stäuble, A., Qiu, T., Kathayat, R. S., Dickinson, B. C., Gärtner, J., Sheldrick, G. M., Krätznner, R., & Steinfeld, R. (2022). Cln5 represents a new type of cysteine-based S-depalmitoylase linked to neurodegeneration. *Science Advances*, 8(15), 1–10. <https://doi.org/10.1126/sciadv.abj8633>
- Mancini, C., Nassani, S., Guo, Y., Chen, Y., Giorgio, E., Brussino, A., Di Gregorio, E., Cavaliere, S., Lo Buono, N., Funaro, A., Pizio, N. R., Nmezi, B., Kytälä, A., Santorelli, F. M., Padiath, Q. S., Hakonarson, H., Zhang, H., & Brusco, A. (2015). Adult-onset autosomal recessive ataxia associated with neuronal ceroid lipofuscinosis type 5 gene (CLN5) mutations. *Journal of Neurology*, 262(1), 173–178. <https://doi.org/10.1007/s00415-014-7553-y>
- Mayhew, I. G., Jolly, R. D., Pickett, B. T., & Slack, P. M. (1985). Ceroid-lipofuscinosis (Batten's disease): Pathogenesis of blindness in the ovine model. *Neuropathology and Applied Neurobiology*, 11(4), 273–290. <https://doi.org/10.1111/j.1365-2990.1985.tb00025.x>
- Meiman, E. J., Kick, G. R., Jensen, C. A., Coates, J. R., & Katz, M. L. (2022). Characterization of neurological disease progression in a canine model of CLN5 neuronal ceroid lipofuscinosis. *Developmental Neurobiology*, 82(4), 326–344. <https://doi.org/10.1002/dneu.22878>
- Mirza, M., Volz, C., Karlstetter, M., Langiu, M., Somogyi, A., Ruonala, M. O., Tamm, E. R., Jäggle, H., & Langmann, T. (2013). Progressive retinal degeneration and glial activation in the CLN6 (nclf) mouse model of neuronal ceroid lipofuscinosis: A beneficial effect of DHA and curcumin supplementation. *PLoS ONE*, 8(10), e75963. <https://doi.org/10.1371/journal.pone.0075963>
- Mitchell, N. L., Russell, K. N., Wellby, M. P., Wicky, H. E., Schoderboeck, L., Barrell, G. K., Melzer, T. R., Gray, S. J., Hughes, S. M., & Palmer, D. N. (2018). Longitudinal in vivo monitoring of CNS demonstrates the efficacy of gene therapy in a sheep model of CLN5 Batten disease. *Molecular Therapy*, 26, 2366–2378. <https://doi.org/10.1016/j.ythm.2018.07.015>
- Mizukami, K., Kawamichi, T., Koie, H., Tamura, S., Matsunaga, S., Imamoto, S., Saito, M., Hasegawa, D., Matsuki, N., Tamahara, S., Sato, S., Yabuki, A., Chang, H.-S., Yamato, O., Landoni, M. F., & Thompson, E. J. (2012). Neuronal ceroid lipofuscinosis in Border Collie dogs in Japan: Clinical and molecular epidemiological study (2000–2011). *The Scientific World Journal*, 2012, 383174. <https://doi.org/10.1100/2012/383174>
- Mohd Ismail, I. F. (2014). Identification of a novel mutation in the CLN6 gene causing neuronal ceroid lipofuscinosis in South Hampshire sheep (PhD thesis). University of Sydney. <http://hdl.handle.net/2123/14579>
- Mole, S. E., Williams, R. E., & Goebel, H. H. (Eds.). (2011). *The neuronal ceroid lipofuscinoses (Batten disease)* (2nd ed.). Oxford University Press.

- Mole, S. E., Michaux, G., Codlin, S., Wheeler, R. B., Sharp, J. D., & Cutler, D. F. (2004). CLN6, which is associated with a lysosomal storage disease, is an endoplasmic reticulum protein. *Experimental Cell Research*, 298(2), 399–406. <https://doi.org/10.1016/j.yexcr.2004.04.042>
- Morgan, J. P., Magee, H., Wong, A., Nelson, T., Koch, B., Cooper, J. D., & Weimer, J. M. (2013). A murine model of variant late infantile ceroid lipofuscinosis recapitulates behavioral and pathological phenotypes of human disease. *PLoS ONE*, 8(11), e78694. <https://doi.org/10.1371/journal.pone.0078694>
- Murray, S. J., Almuqbel, M. M., Felton, S. A., Palmer, N. J., Myall, D. J., Shoorangiz, R., Ella, A., Keller, M., Palmer, D. N., Melzer, T. R., & Mitchell, N. L. (2022). Progressive MRI brain volume changes in ovine models of CLN5 and CLN6 neuronal ceroid lipofuscinosis. *Brain Communications*, 5(1), fcac33900. <https://doi.org/10.1093/braincomms/fcac339>
- Nita, D. A., Mole, S. E., & Minassian, B. A. (2016). Neuronal ceroid lipofuscinoses. *Epileptic Disorders*, 18, 73–88. <https://doi.org/10.1684/epd.2016.0844>
- Oswald, M. J., Palmer, D. N., Kay, G. W., Barwell, K. J., & Cooper, J. D. (2008). Location and connectivity determine GABAergic interneuron survival in the brains of South Hampshire sheep with CLN6 neuronal ceroid lipofuscinosis. *Neurobiology of Disease*, 32(1), 50–65. <https://doi.org/10.1016/j.nbd.2008.06.004>
- Oswald, M. J., Palmer, D. N., Kay, G. W., Shemilt, S. J. A., Rezaie, P., & Cooper, J. D. (2005). Glial activation spreads from specific cerebral foci and precedes neurodegeneration in presymptomatic ovine neuronal ceroid lipofuscinosis (CLN6). *Neurobiology of Disease*, 20(1), 49–63. <https://doi.org/10.1016/j.nbd.2005.01.025>
- Palmer, D. N. (2015). The relevance of the storage of subunit c of ATP synthase in different forms and models of Batten disease (NCLs). *Biochimica et Biophysica Acta*, 1852(10), 2287–2291. <https://doi.org/10.1016/j.bbadis.2015.06.014>
- Peña, J. A., Cardozo, J. J., Montiel, C. M., Molina, O. M., & Boustany, R. (2001). Serial MRI findings in the Costa Rican variant of neuronal ceroid-lipofuscinosis. *Pediatric Neurology*, 25(1), 78–80. [https://doi.org/10.1016/s0887-8994\(01\)00284-3](https://doi.org/10.1016/s0887-8994(01)00284-3)
- Russell, K. N., Mitchell, N. L., Anderson, N. G., Bunt, C. R., Wellby, M. P., Melzer, T. R., Barrell, G. K., & Palmer, D. N. (2018). Computed tomography provides enhanced techniques for longitudinal monitoring of progressive intracranial volume loss associated with regional neurodegeneration in ovine neuronal ceroid lipofuscinoses. *Brain and Behavior*, 8(9), e01096. <https://doi.org/10.1002/brb3.1096>
- Russell, K. N., Mitchell, N. L., Wellby, M. P., Barrell, G. K., & Palmer, D. N. (2021). Electroretinography data from ovine models of CLN5 and CLN6 neuronal ceroid lipofuscinoses. *Data in Brief*, 37, 107188. <https://doi.org/10.1016/j.dib.2021.107188>
- Sawiak, S. J., Perumal, S. R., Rudiger, S. R., Matthews, L., Mitchell, N. L., McLaughlan, C. J., Bawden, C. S., Palmer, D. N., Kuchel, T., & Morton, A. J. (2015). Rapid and progressive regional brain atrophy in CLN6 Batten disease affected sheep measured with longitudinal magnetic resonance imaging. *PLoS ONE*, 10(7), e0132331. <https://doi.org/10.1371/journal.pone.0132331>
- Schulz, A., Ajayi, T., Specchio, N., de Los Reyes, E., Gissen, P., Ballon, D., Dyke, J. P., Cahan, H., Slasor, P., Jacoby, D., & Kohlschütter, A. (2018). Study of intraventricular cerliponase alfa for CLN2 disease. *New England Journal of Medicine*, 378(20), 1898–1907. <https://doi.org/10.1056/NEJMoa1712649>
- Simonati, A., Williams, R. E., Nardocci, N., Laine, M., Battini, R., Schulz, A., Garavaglia, B., Moro, F., Pezzini, F., & Santorelli, F. M. (2017). Phenotype and natural history of variant late infantile ceroid-lipofuscinosis 5. *Developmental Medicine and Child Neurology*, 59(8), 815–821. <https://doi.org/10.1111/dmcn.13473>
- Singh, V. K., & Seed, T. M. (2021). How necessary are animal models for modern drug discovery? *Expert Opinion on Drug Discovery*, 16(12), 1391–1397. <https://doi.org/10.1080/17460441.2021.1972255>
- Tammen, I., Cook, R. W., Nicholas, F. W., & Raadsma, H. W. (2001). Neuronal ceroid lipofuscinosis in Australian Merino sheep: A new animal model. *European Journal of Paediatric Neurology*, 5(Suppl.A), 37–41. <https://doi.org/10.1053/ejpn.2000.0432>
- Tammen, I., Houweling, P. J., Frugier, T., Mitchell, N. L., Kay, G. W., Cavanagh, J. A. L., Cook, R. W., Raadsma, H. W., & Palmer, D. N. (2006). A missense mutation (c.184C>T) in ovine CLN6 causes neuronal ceroid lipofuscinosis in Merino sheep whereas affected South Hampshire sheep have reduced levels of CLN6 mRNA. *Biochimica et Biophysica Acta*, 1762(10), 898–905. <https://doi.org/10.1016/j.bbadis.2006.09.004>
- Tyynelä, J., Suopanki, J., Santavuori, P., Baumann, M., & Haltia, M. (1997). Variant late infantile neuronal ceroid-lipofuscinosis: Pathology and biochemistry. *Journal of Neuropathology and Experimental Neurology*, 56(4), 369–375. <https://doi.org/10.1097/00005072-199704000-00005>
- Westlake, V. J., Jolly, R. D., Jones, B. R., Mellor, D. J., Machon, R., Zanjani, E. D., & Krivit, W. (1995). Hematopoietic cell transplantation in fetal lambs with ceroid-lipofuscinosis. *American Journal of Medical Genetics*, 57(2), 365–368. <https://doi.org/10.1002/ajmg.1320570252>

SUPPORTING INFORMATION

Additional supporting information can be found online in the Supporting Information section at the end of this article.

How to cite this article: Mitchell, N. L., Russell, K. N., Barrell, G. K., Tammen, I., & Palmer, D. N. (2023). Characterization of neuropathology in ovine CLN5 and CLN6 neuronal ceroid lipofuscinoses (Batten disease). *Developmental Neurobiology*, 1–16. <https://doi.org/10.1002/dneu.22918>